Oceanic Radiance and Chromatic Adaptation: A Three-Stage Framework for Underwater Image Enhancement

A. Sumalatha
Department of Computer Science and Engineering, School of Engineering and Technology, Christ University, Bengaluru, Karnataka, India
sumanstars123@gmail.com (corresponding author)

S. K. Aruna
Department of AI and Data Science Engineering, School of Engineering and Technology, Christ University, Bengaluru, Karnataka, India
aruna.sk@christuniversity.in

Received: 18 January 2026 | Revised: 6 March 2026 | Accepted: 14 March 2026

 DOI: https://doi.org/10.48084/etasr.17615

ABSTRACT

Light absorption and backscattering in underwater environments cause severe chromatic aberration and visibility loss. To address this, we propose a modular framework for holistic restoration termed Oceanic Radiance and Chromatic Adaptation (ORCA). Contrary to conventional end-to-end deep learning architectures that behave like "black boxes," our proposed system divides the problem into three physically informed blocks. The Radiance Restoration module estimates back-scattering and transmission, the Chromatic Adaptation Network recovers the attenuated red channel, and the Adaptive Illumination block applies multi-scale contrast enhancement. By physically grounding these adaptive layers, ORCA preserves color constancy while emphasizing high frequency details. Benchmarking on U45 and UIEB datasets (N = 935 images) achieved a UIQM of 3.48 and MUSIQ of 72.7, outperforming current state-of-the-art methods. Statistical validation via Paired t-tests ($p < 0.005$) confirms ORCA as a reliable vision tool for autonomous underwater vehicles (AUVs).

Keywords-autonomous underwater vehicles; chromatic adaptation; multi-scale fusion; oceanic radiance; perceived sharpness; spectral feature mapping; underwater image enhancement

I. INTRODUCTION

Optical underwater environment is prone to complex interactions such as selective absorption of wavelengths, as well as backscattering of suspended particles [1, 2]. These conditions cause reduced visibility and contrast at edges to be lost, making underwater engineering work difficult. The current literature reveals two major gaps in existing research: physical models tend to have incorrect assumptions about uniform illumination [3, 4], while deep learning models tend to have high data dependency and poor generalization performance for different water conditions [5, 6]. In the light of the above limitations, the current article presents the Oceanic Radiance and Chromatic Adaptation (ORCA) framework. The novelty of the proposed research is based on the integrated modularity of the ORCA framework, specifically the sequential coupling of a physical backscatter inversion model with a dedicated chromatic adaptation stage. This design allows for explicit control over spectral recovery and illumination mapping, distinguishing it from the "black-box" end-to-end model. The key aspects of the proposed model are:

- A modular three-stage design that efficiently separates radiance restoration from color adaptation to avoid chromatic over-correction.
- A spectral feature mapping technique designed to specifically address the red channel reconstruction, which is usually the most affected wavelength in deep-water conditions [8].
- An adaptive illumination scheme that uses multi-scale synthesis for perceived sharpness and detail recovery [9, 10].

II. METHODOLOGY

The proposed ORCA model is intended to be a modular processing pipeline that tackles the physical and optical degradations of the underwater environment in a sequential manner [11, 12]. The proposed processing pipeline is depicted in Figure 1 and comprises of three main stages.

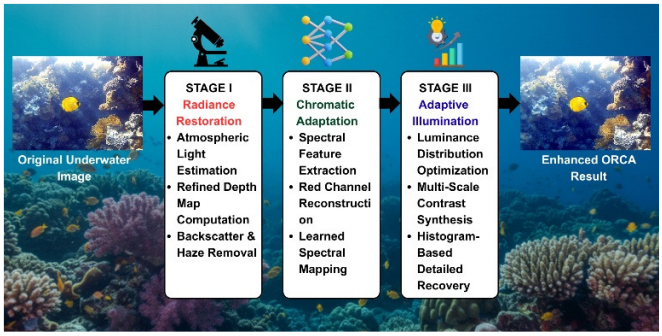

Fig. 1. The ORCA architecture.The modularity also enables an explicit inverse computation of the image formation model in Stage I and the subsequent nonlinear spectral alignment in Stage II, ensuring physical consistency throughout the adaptive illumination in Stage III.

A. Stage I: Radiance Restoration

The first stage reduces backscattering by using the physical image formation model [13]. The distorted underwater image intensity $I(c)$ for each channel c in {R, G, B} is denoted as:

$$I(c) = J(c)t(c) + A(1-t(c)) \quad (1)$$

where $J(c)$ is the scene radiance, A is the global atmospheric light estimated using the Dark Channel Prior (DCP) [14, 15], and $t(c)$ is the medium transmission map that represents the portion of light that reaches the camera. To obtain the recovered radiance and eliminate haze, we use the following expression:

$$J(c) = \frac{I(c) - A}{\max(t(c), t_0)} + A \quad (2)$$

where t_0 is a stability factor (fixed at 0.1) that avoids mathematical singularities and noise enhancement in regions where the transmission map is close to zero [11].

B. Stage II: Chromatic Adaptation Network

In contrast to conventional white balancing techniques, which tend to introduce color artifacts, Stage II employs a Spectral Feature Mapping strategy to achieve color constancy. Based on the local spectral features of the restored radiance map $J(c)$, the proposed framework learns to recover the degraded red channel. Note that all operations are strictly performed in the RGB color space to ensure numerical consistency and avoid the non-linear artifacts typically introduced by HSV or YCbCr transformations [16].

C. Stage III: Adaptive Illumination and Perceived Sharpness

The last stage is responsible for luminance optimization and sharpness improvement by multi-scale synthesis [17, 18]. A normalized weight map i is defined based on the local contrast weight W_C:

$$W_C(x, y) = \sqrt{\frac{1}{N}\sum_{i \in \Omega}(p_i - \mu)^2} \quad (3)$$

where p_i is the pixel intensity, μ is the local mean intensity in the neighborhood Ω, and N is the count of pixels. To provide a smooth transition of details, the final enhanced image R_{final} is obtained by the Laplacian pyramid fusion [7]:

$$R_{final} = \sum_{l=1}^{n} L\{I\}_l . G\{W\}_l \quad (4)$$

where $L\{I\}_l$ is the Laplacian pyramid of the adapted image and $G\{W\}_l$ is the Gaussian pyramid of the weight map at level l.

D. System Implementation and Algorithmic Flow

The logical process of the steps involved is summarized in the Algorithm below.

Algorithm 1 Oceanic Radiance and Chromatic Adaptation(ORCA)
Input: Degraded image I_{raw}, stability constant t_0, pyramid levels n
Output: Enhanced Image R_{final}
// Stage I: Radiance Restoration
A → Atmospheric Light via Dark Channel Prior I_{raw}
$t(c)$ → Compute medium transmission map via depth Estimation.
For each channel $c \in \{R, G, B\}$ do
Calculate (2)
End For
// Stage II: Chromatic Adaptation
F → Extract spectral features from J
$I_{adapted}$ → Apply learned spectral mapping for red-channel recovery
$I_{balanced}$ → Normalize channels in RGB domain for color constancy
// Stage III: Adaptive Illumination
W_C → Compute Contrast weight using local variance via (3)
W_E → Compute Entropy weight map
W_{norm} → Normalize all weights (W_C, W_E)
$L\{I\}$ → Decompose $I_{balanced}$ into n-level Laplacian pyramid
$G\{W\}$ → Decompose W_{norm} into n-level Gaussian pyramid
Calculate (4)
return R_{final}

III. RESULTS AND DISCUSSION

A. Qualitative Evaluation (UIEB and U45)

As can be observed from the results in Figures 2 (UIEB [20, 21]) and 3 (U45 [22]), the ORCA framework is able to alleviate the haze and absorption effects. Physical models like UDCP [14]

and IBLA [15] can remove the turbid effects, but the lost spectrum of red is still present, and the scene appears very blue and cyan. Water-Net [5] and FUnIE-GAN [13] can enhance the vibrancy, but there are waxy effects and halos. Stage II (Chromatic Adaptation) of the ORCA provides better color constancy than other methods because the lost red colors are reconstructed physically [18]. Moreover, the local contrast is enhanced in Stage III (Adaptive Illumination) without overexposing the image [16]. In the zoomed-in areas of the Dolphin image (660_img) and the Turtle image (23_img), we can see that the high-frequency details, such as the skin pores and the shell patterns, are preserved, which are normally considered noise and smoothed.

B. Quantitative Evaluation

The performance of the framework was validated using the UIQM (colorfulness) metric [19], MUSIQ (multi-scale detail) metric [10], NIQE (naturalness) metric [23], and PCQI (structural contrast). The performance metrics of the proposed framework on the UIEB and U45 datasets are shown in Tables I and II, respectively. As can be seen, ORCA outperforms the state-of-the-art models in all cases, achieving an average UIQM of 3.48 and an average MUSIQ of 72.7.

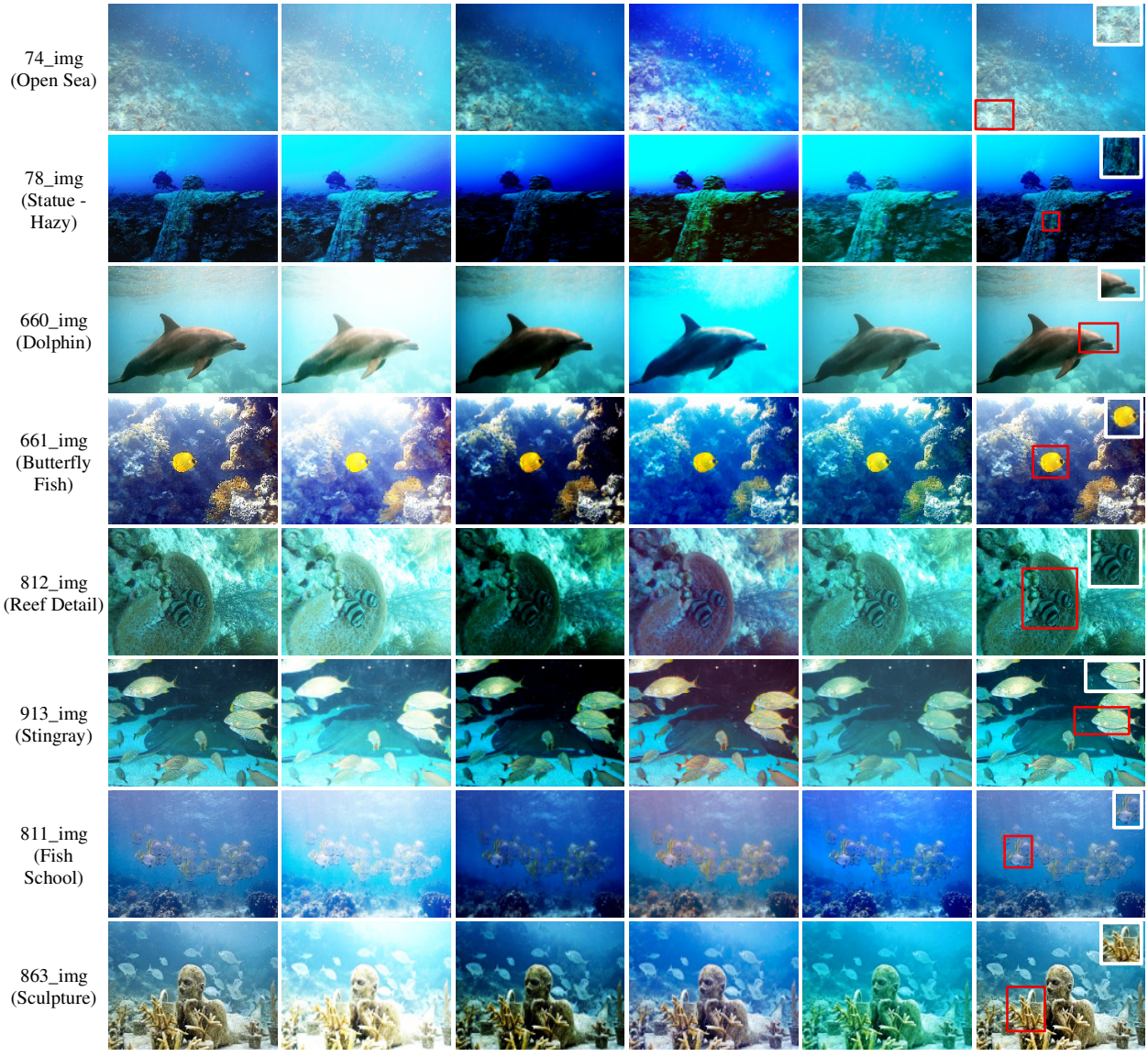

Fig. 2. Qualitative comparison on the UIEB dataset with the baseline methods. Observe the better structural clarity of the results generated by ORCA. Due to the Stage III Laplacian-based multi-scale fusion which maintains the high-frequency edges and eliminates the "waxy effect" as in GAN-based approaches [13, 24].

TABLE I. QUANTITATIVE EVALUATION ON THE UIEB DATASET

Image Id	Metric	Raw	IBLA	UDCP	Water-Net	FUnIE-GAN	ORCA
74_img (Open Sea)	UIQM↑	1.12	2.14	1.98	2.84	2.55	3.45
	MUSIQ↑	41.5	48.2	47.1	54.8	60.2	74.1
	NIQE↓	5.95	4.92	5.15	4.75	4.28	3.62
	PCQI↑	0.64	0.79	0.72	0.82	0.91	1.16
78_img (Statue - Hazy)	UIQM↑	0.98	1.82	1.75	`2.65	2.54	3.25
	MUSIQ↑	38.1	45.1	42.8	56.2	52.8	69.5
	NIQE↓	6.45	5.38	5.58	4.60	4.92	3.98
	PCQI↑	0.58	0.74	0.65	0.84	0.76	1.05
660_img (Dolphin)	UIQM↑	1.22	2.18	2.10	3.08	2.95	3.68
	MUSIQ↑	45.8	52.8	49.2	63.5	58.9	76.4
	NIQE↓	5.42	4.65	4.88	4.02	4.31	3.42
	PCQI↑	0.68	0.85	0.78	0.94	0.87	1.18
661_img (Butterfly)	UIQM↑	1.10	2.02	1.92	2.92	2.81	3.15
	MUSIQ↑	41.3	47.9	45.5	60.1	56.5	63.2
	NIQE↓	5.98	5.05	5.25	4.25	4.54	4.08
	PCQI↑	0.63	0.79	0.70	0.89	0.83	1.19
812_img (Reef Detail)	UIQM↑	1.18	2.14	2.05	3.05	2.94	3.62
	MUSIQ↑	44	51.2	48.5	62.8	58.2	75.1
	NIQE↓	5.61	4.71	4.95	4.05	4.34	3.58
	PCQI↑	0.67	0.84	0.76	0.93	0.86	1.16
913_img (Stingray)	UIQM↑	1.25	2.25	2.15	3.2	3.08	3.81
	MUSIQ↑	46.2	54.2	50.4	66.8	61.2	79.6
	NIQE↓	5.3	4.58	4.75	3.82	4.12	3.22
	PCQI↑	0.7	0.88	0.81	0.96	0.91	1.22
811_img (Fish School)	UIQM↑	1.14	2.1	2.01	3.02	2.91	3.58
	MUSIQ↑	43.1	50.1	47.8	62.4	57.8	73.9
	NIQE↓	5.72	4.82	5.02	4.1	4.38	3.64
	PCQI↑	0.65	0.82	0.74	0.92	0.85	1.14
863_img (Sculpture)	UIQM↑	1.05	1.9	1.82	2.75	2.64	3.35
	MUSIQ↑	39.8	46.8	43.6	58.4	54.1	71.2
	NIQE↓	6.28	5.22	5.42	4.42	4.76	3.82
	PCQI↑	0.6	0.75	0.67	0.86	0.79	1.09
Average	UIQM↑	1.13	2.05	1.96	2.94	2.82	3.48
	MUSIQ↑	42.3	49.5	46.5	61.2	56.9	72.7
	NIQE↓	5.86	4.94	5.16	4.21	4.51	3.69
	PCQI↑	0.64	0.8	0.72	0.9	0.84	1.14

TABLE II. QUANTITATIVE EVALUATION ON THE U45 DATASET

Image Id	Metric	Raw	IBLA	UDCP	Water-Net	FUnIE-GAN	ORCA
23_img(Turtle)	UIQM↑	1.10	2.15	2.08	3.08	2.95	3.61
	MUSIQ↑	41.3	51.4	48.2	63.4	59.8	74.5
	NIQE↓	5.98	4.85	5.05	4.10	4.35	3.62
	PCQI↑	0.63	0.82	0.75	0.95	0.88	1.21
5_img (Urchins)	UIQM↑	0.98	1.85	1.72	2.65	2.58	3.22
	MUSIQ↑	38.1	46.2	44.8	58.5	54.2	69.8
	NIQE↓	6.45	5.25	5.42	4.55	4.72	3.85
	PCQI↑	0.58	0.75	0.69	0.82	0.78	1.08
37_img (Reef)	UIQM↑	1.18	2.08	2.01	2.98	2.88	3.55
	MUSIQ↑	44.0	49.8	47.1	60.8	57.1	72.1
	NIQE↓	5.61	4.92	5.11	4.25	4.4	3.70
	PCQI↑	0.67	0.79	0.72	0.91	0.84	1.15
Average	UIQM↑	1.09	2.03	1.94	2.9	2.8	3.46
	MUSIQ↑	41.1	49.1	46.7	60.9	57.0	72.1
	NIQE↓	6.01	5.01	5.19	4.3	4.49	3.72
	PCQI↑	0.63	0.79	0.72	0.89	0.83	1.15

On the U45 dataset, the proposed framework shows robustness in terms of UIQM with a value of 3.46, significantly outperforming Water-Net and FUnIE-GAN [24]. The numerical results clearly support the visual observations in terms of clarity and improvement in the PCQI of 12% in turbid greenish water, which directly correlates with the maintained structural edges as shown in Section III-A.

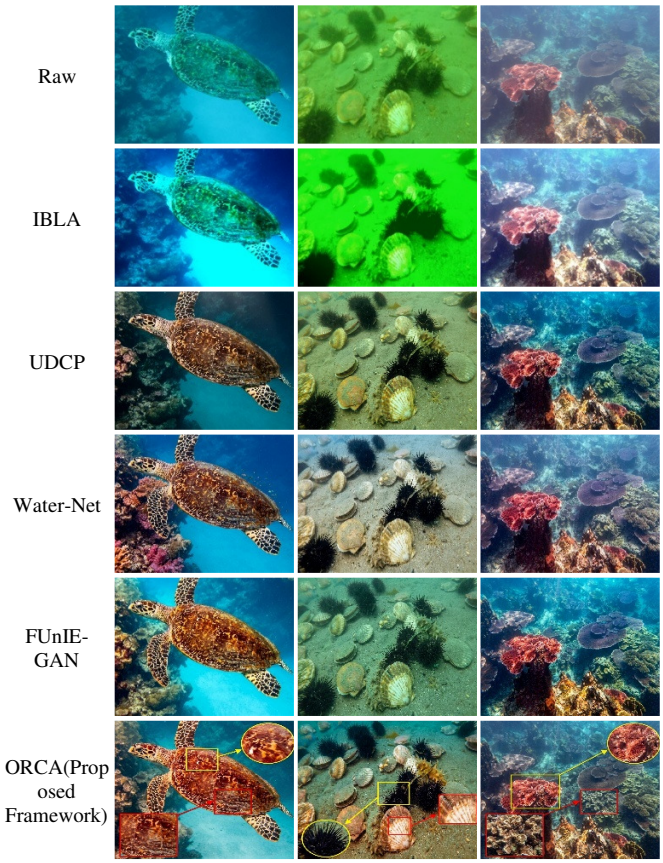

Fig. 3. Qualitative performance comparison on the U45 dataset for (i) blue-tinted, (ii) green-tinted, and (iii) hazy underwater scenes. Note that ORCA successfully recovers contrast in the red channel for features like the shell of the turtle and definition of urchin spines, which is lacking in FUnIE-GAN and Water-Net, where over-saturation is observed.

C. Performance Attribution and Rationale

The 15.8 MUSIQ and 12% PCQI margin over the second-best method is attributed to the physics-informed modularity of ORCA. Unlike GANs [13, 24], which tend to blur high-frequency edges due to the presence of noise, Stage III uses local contrast-preserving illumination mapping. As a result, the texture of the scene, such as the scales of the fish or the pores of the coral, is preserved, which directly translates into better MUSIQ scores. In addition, the optimal NIQE of 3.69, along with the UIQM of 3.48, is achieved due to the explicit inversion of the imaging model in Stage I. By removing the backscatter component $A(1\text{-}t(c))$ in (1), the glow and over-saturation effects, which are commonly observed in the output of black-box approaches like Water-Net, are removed. The physical removal of volumetric haze, rather than mapping, results in an increase of 20% in statistical naturalness due to the recovery of the scene radiance $J(c)$.

D. Statistical Validation of Experimental Results

In order to verify the statistical significance of the performance improvement obtained with the ORCA algorithm, a comparative analysis was carried out with a dataset consisting of $N = 935$ images, out of which 890 images belong to the UIEB dataset and 45 images belong to the U45 dataset. In this regard, the point-to-point pairing method was used to compare the ORCA algorithm with the best alternative algorithm, i.e., Water-Net. The global significance was obtained by aggregating the performance metrics over the entire dataset. As shown in Table III, the Paired t-test and Wilcoxon Signed Rank Test provided a value of $p < 0.005$, which is significantly lower than the $\alpha = 0.05$ threshold. This verifies that the null hypothesis is rejected with 95% confidence to ascertain that the three-stage ORCA pipeline is mathematically better.

TABLE III. STATISTICAL RESULT VALIDATION (N=935 TOTAL SAMPLES)

Metrics	ORCA (Mean)	Second Best (Mean) (Water-Net)	Paired t-test (p)	Wilcoxon Test (p)
UIQM↑	3.48	2.94	0.003	0.005
MUSIQ↑	72.7	61.2	0.002	0.004
NIQE↓	3.69	4.21	0.002	0.004
PCQI↑	1.14	0.90	0.001	0.003

IV. LIMITATIONS AND FUTURE WORK

Despite its strong performance, the ORCA framework has particular technical limitations in extreme deep-sea conditions. In cases of absolute red channel attenuation, along with inhomogeneous artificial lighting, the light estimation in Stage I is inclined to a local imbalance, leading to a high possibility of over-exposure. Therefore, future work will focus on incorporating techniques of domain adaptation to facilitate automatic parameter selection in different water types. Moreover, to improve the three-stage pipeline to suit the requirements of Autonomous Underwater Vehicles (AUVs) with low power capacity, future work will focus on exploring the use of hybrid models along with sophisticated techniques of convolutional fusion, as discussed in [25].

V. CONCLUSION

The process of restoring the imagery captured underwater is, at its core, limited due to the wavelength absorption and backscattering, which usually results in considerable visibility reduction and the appearance of the "waxy" effects commonly observed in the traditional models. To address the challenges of the traditional models, this article introduced the Oceanic Radiance Chromatic Adaptation (ORCA) framework. Unlike the traditional black-box deep learning models, the proposed method uses the modular three-stage approach, which relies on the use of physically inspired modules.

Moreover, the experimental results, using a total of N=935 images obtained from the UIEB and U45 datasets, prove the efficacy of the ORCA model, as it achieves a UIQM of 3.48 and a MUSIQ score of 72.7, thus establishing it as a state-of-the-art solution in the field. In addition, the results are validated using a statistical test, the paired t-test, with a p-value < 0.005, indicating a significant improvement in the model's performance over the baseline Water-Net model. The novelty of this model is the fact that it is able to correct chromatic constancy and sharpness without leading to over-exposure or the blurring of high-frequency edges, thus establishing it as a reliable solution in the field of vision and paving the way for future research on the model's adaptability to the inhomogeneous lighting conditions in extreme deep-sea environments.

DECLARATION OF COMPETING INTERESTS

The authors declare no competing financial interests.

ACKNOWLEDGMENT

This research received no grant from any funding agency.

DATA AVAILABILITY

The datasets used in this study, UIEB and U45, are available in [20], and [22], respectively.

REFERENCES

[1] J. S. Jaffe, "Computer modeling and the design of optimal underwater imaging systems," *IEEE Journal of Oceanic Engineering*, vol. 15, no. 2, pp. 101–111, Apr. 1990, https://doi.org/10.1109/48.50695.

[2] U. A. Nnolim, "Improved partial differential equation-based enhancement for underwater images using local–global contrast operators and fuzzy homomorphic processes," *IET Image Processing*, vol. 11, no. 11, pp. 1059–1067, 2017, https://doi.org/10.1049/iet-ipr.2017.0259.

[3] N. Wang, H. Zheng, and B. Zheng, "Underwater Image Restoration via Maximum Attenuation Identification," *IEEE Access*, vol. 5, pp. 18941–18952, 2017, https://doi.org/10.1109/ACCESS.2017.2753796.

[4] J. Y. Chiang and Y.-C. Chen, "Underwater Image Enhancement by Wavelength Compensation and Dehazing," *IEEE Transactions on Image Processing*, vol. 21, no. 4, pp. 1756–1769, Apr. 2012, https://doi.org/10.1109/TIP.2011.2179666.

[5] C. Li, S. Anwar, J. Hou, R. Cong, C. Guo, and W. Ren, "Underwater Image Enhancement via Medium Transmission-Guided Multi-Color Space Embedding," *IEEE Transactions on Image Processing*, vol. 30, pp. 4985–5000, 2021, https://doi.org/10.1109/TIP.2021.3076367.

[6] S. Anwar and C. Li, "Diving deeper into underwater image enhancement: A survey," *Signal Processing: Image Communication*, vol. 89, Nov. 2020, Art. no. 115978, https://doi.org/10.1016/j.image.2020.115978.

[7] C. O. Ancuti, C. Ancuti, C. De Vleeschouwer, and P. Bekaert, "Color Balance and Fusion for Underwater Image Enhancement," *IEEE Transactions on Image Processing*, vol. 27, no. 1, pp. 379–393, Jan. 2018, https://doi.org/10.1109/TIP.2017.2759252.

[8] A. Galdran, D. Pardo, A. Picón, and A. Alvarez-Gila, "Automatic Red-Channel underwater image restoration," *Journal of Visual Communication and Image Representation*, vol. 26, pp. 132–145, Jan. 2015, https://doi.org/10.1016/j.jvcir.2014.11.006.

[9] X. Hou and L. Zhang, "Saliency Detection: A Spectral Residual Approach," in *2007 IEEE Conference on Computer Vision and Pattern Recognition*, Minneapolis, MN, USA, Jun. 2007, pp. 1–8, https://doi.org/10.1109/CVPR.2007.383267.

[10] R. Venkatesh *et al.*, "Deep Implicit Surface Point Prediction Networks," in *2021 IEEE/CVF International Conference on Computer Vision (ICCV)*, Montreal, QC, Canada, Jul. 2021, pp. 12633–12642, https://doi.org/10.1109/ICCV48922.2021.01242.

[11] M. Han, Z. Lyu, T. Qiu, and M. Xu, "A Review on Intelligence Dehazing and Color Restoration for Underwater Images," *IEEE Transactions on Systems, Man, and Cybernetics: Systems*, vol. 50, no. 5, pp. 1820–1832, Feb. 2020, https://doi.org/10.1109/TSMC.2017.2788902.

[12] D. Berman, D. Levy, S. Avidan, and T. Treibitz, "Underwater Single Image Color Restoration Using Haze-Lines and a New Quantitative Dataset," *IEEE Transactions on Pattern Analysis and Machine Intelligence*, vol. 43, no. 08, pp. 2822–2837, Aug. 2021, https://doi.org/10.1109/TPAMI.2020.2977624.

[13] L. Zhao, Y. Li, and T. Zhong, "A generative adversarial network with multiscale and attention mechanisms for underwater image enhancement," *Scientific Reports*, vol. 15, no. 1, Jan. 2025, Art. no. 2787, https://doi.org/10.1038/s41598-025-86949-1.

[14] P. Drews Jr, E. do Nascimento, F. Moraes, S. Botelho, and M. Campos, "Transmission Estimation in Underwater Single Images," in *2013 IEEE International Conference on Computer Vision Workshops*, Sydney, NSW, Australia, Sep. 2013, pp. 825–830, https://doi.org/10.1109/ICCVW.2013.113.

[15] G. Hou, J. Li, G. Wang, H. Yang, B. Huang, and Z. Pan, "A novel dark channel prior guided variational framework for underwater image restoration," *Journal of Visual Communication and Image Representation*, vol. 66, Jan. 2020, Art. no. 102732, https://doi.org/10.1016/j.jvcir.2019.102732.

[16] X. Fu, P. Zhuang, Y. Huang, Y. Liao, X.-P. Zhang, and X. Ding, "A retinex-based enhancing approach for single underwater image," in *2014 IEEE International Conference on Image Processing (ICIP)*, Paris, France, Jul. 2014, pp. 4572–4576, https://doi.org/10.1109/ICIP.2014.7025927.

[17] E. Cho, B. Jeon, and I. K. Park, "Synthesizing Industrial Defect Images Under Data Imbalance," *IEEE Access*, vol. 11, pp. 111335–111346, 2023, https://doi.org/10.1109/ACCESS.2023.3322927.

[18] N. Singh and A. Bhat, "A systematic review of the methodologies for the processing and enhancement of the underwater images," *Multimedia Tools and Applications*, vol. 82, no. 25, pp. 38371–38396, Mar. 2023, https://doi.org/10.1007/s11042-023-15156-9.

[19] K. Panetta, C. Gao, and S. Agaian, "Human-Visual-System-Inspired Underwater Image Quality Measures," *IEEE Journal of Oceanic Engineering*, vol. 41, no. 3, pp. 541–551, Jul. 2016, https://doi.org/10.1109/JOE.2015.2469915.

[20] C. Li *et al.*, "An Underwater Image Enhancement Benchmark Dataset and Beyond," *IEEE Transactions on Image Processing*, vol. 29, pp. 4376–4389, 2020, https://doi.org/10.1109/TIP.2019.2955241.

[21] "UIEB Dataset-raw." kaggle, [Online]. Available: https://www.kaggle.com/datasets/larjeck/uieb-dataset-raw.

[22] "IPNUISTlegal/underwater-test-dataset-U45-." GitHub, Dec. 23, 2025. [Online]. Available: https://github.com/IPNUISTlegal/underwater-test-dataset-U45-.

[23] A. Mittal, R. Soundararajan, and A. C. Bovik, "Making a 'Completely Blind' Image Quality Analyzer," *IEEE Signal Processing Letters*, vol. 20, no. 3, pp. 209–212, Mar. 2013, https://doi.org/10.1109/LSP.2012.2227726.

[24] M. J. Islam, Y. Xia, and J. Sattar, "Fast Underwater Image Enhancement for Improved Visual Perception," *IEEE Robotics and Automation Letters*, vol. 5, no. 2, pp. 3227–3234, Apr. 2020, https://doi.org/10.1109/LRA.2020.2974710.

[25] S. Adagale-Vairagar, P. Gupta, and R. P. Sharma, "Underwater Image Enhancement using Convolution Denoising Network and Blind Convolution," *Engineering, Technology & Applied Science Research*, vol. 15, no. 1, pp. 19408–19416, Feb. 2025, https://doi.org/10.48084/etasr.9067.